Materials and Design 201 (2021) 109460

Contents lists available at ScienceDirect

Materials and Design

journal homepage: www.elsevier.com/locate/matdes

Fabrication and characterization of carbon foams using 100% Kraft lignin

Qiangu Yan [a], Rachel Arango [b], Jinghao Li [b], Zhiyong Cai [b,*]

[a] Ligwood LLC, Madison, WI 53705, USA
[b] Forest Products Laboratory, One Gifford Pinchot Drive, Madison, WI 53726-2398, USA

HIGHLIGHTS

- Open cell carbon foams were prepared from 100% Kraft lignin under atmospheric pressure.
- No catalysts, blowing agents, surfactants were used for the foam preparation.
- Carbon foams demonstrated high mechanical properties.
- Carbon foams exhibited excellent fire resistance.
- Termite testing showed no degradation to carbon foam after the evaluation.

GRAPHICAL ABSTRACT

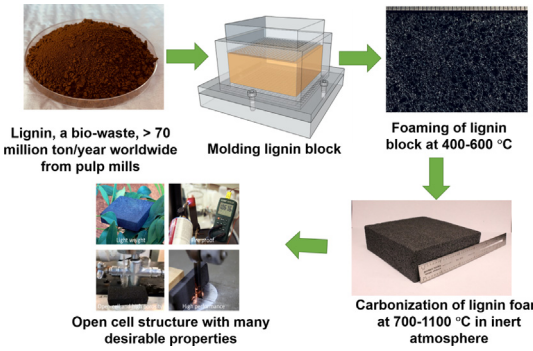

ARTICLE INFO

Article history:
Received 16 October 2020
Received in revised form 4 January 2021
Accepted 7 January 2021
Available online 11 January 2021

Keywords:
Carbon foams
Kraft lignin
Compressive strength
Thermal conductivity
Fire resistance
Termite susceptibility

ABSTRACT

Carbon foams have been prepared using Kraft lignin as the solely resource. No catalysts, foaming/blowing agents, surfactants, and/or crosslinking agents are used for the foam preparation. The process includes pressing carbon foam precursors into molds followed by formation of lignin foam through heating and carbonization/graphitization of the lignin derived foams. The resultant lignin carbon foam (LCF) has an open-cell structure with densities ranging from about 0.18 g/cm^3 to 0.68 g/cm^3. The compressive strengths of LCFs increase with increasing of bulk density, from 7.03 ± 1.25 MPa of LCF1 to 30.16 ± 2.41 MPa of LCF7, and thermal conductivity is strongly influenced by the bulk density with increase from 0.21 ± 0.02 W/(m·K) to 0.75 ± 0.01 W/(m·K). The bulk electrical conductivities of LCF samples increase with increasing of bulk densities from 701 S/m to 2031 S/m. The LCF samples were evaluated for resistance to fire and native subterranean termites. LCF samples exhibit excellent fire resistance, no damage occurred when the LCF sample was exposed to an oxyacetylenic flame in air over 1050 °C for more than 3 min. Termite testing showed no degradation to the LCF samples after the evaluation.

1. Introduction

Lignin is one of the major components of lignocellulosic biomass and the most important natural phenolic polymer. It is a wood by-product composed of 60-65 wt% carbon with an annual production over 70 million tons worldwide from the paper and pulping industries [1]. Much research has been done on the processes involving lignin thermal decomposition to sustainable/renewable carbon-based materials like active carbons, carbon fibers, templated carbon, and graphene [2], but less work has been done on carbon foam production from lignin. Mansmann and Winter [3] developed a process to produce carbon foam from an aqueous lignin solution. However, only ligninsulfonates were used as the lignin precursors, polyethylene oxide and acrylic acid-acrylamide were added as the copolymer, and tremendous energy was consumed to vaporize water from the ligninsulfonate solution in the heating process. Spradling and Amie [4] described a process to produce carbon foam from lignosulfonate. The lignin resource was limited to lignosulfonates in both previous works [3,4] while Kraft lignin, which comprises 95% of the lignin produced annually, was not used

* Corresponding author.
E-mail address: zhiyong.cai@usda.gov (Z. Cai).

https://doi.org/10.1016/j.matdes.2021.109460

for carbon foam production [5]. Currently, carbon foams are mainly produced by the process of blowing the carbon precursors, which are usually first decomposed in a closed vessel at high temperature, under high pressure [6]. This accounts for the high cost of the product since high temperature and high-pressure facilities are required for production. Furthermore, the product size and properties are limited by the facility [7]. Furthermore, catalysts, foaming/blowing agents, surfactants, and/or crosslinking agents may be used for the foam preparation [8], this further increases the cost of the product.

This work reports a simple manufacturing process to produce carbon foams in an open vessel using Kraft lignin as the only carbon precursor; no solvents, catalysts, blowing agents, surfactants, and crosslinking copolymers are needed in this developed method. The properties of Kraft lignin, pretreatment lignin samples, and carbon foams were studied using Fourier transform infrared spectroscopy (FTIR), thermogravimetric analyzer (TGA), X-ray diffractometer (XRD), scanning electron microscope (SEM) and universal testing machine. A possible Kraft lignin foaming and stabilization mechanism was proposed. The densities, mechanical properties, thermal properties and conductivities, chemical compositions, and crystallinity of these carbon foams were analyzed in this study. As these wood-based products are potential building materials, fire and termite resistance of LCF samples were also evaluated.

2. Experimental

2.1. Preparation of lignin carbon foams (LCFs)

A process for fabrication of carbon foams from Kraft lignin was developed, consisting of three steps: molding of lignin block, foaming of lignin block and carbonization of lignin foam (Scheme 1).

Fresh Kraft lignin (labeled as ingredient A) was first heated in a muffle furnace at 450 °C under an inert atmosphere. The temperature was raised from room temperature to 450 °C at a heating rate of 5 °Cmin^{-1} which was maintained for 1 h. The obtained lignin sample was then ground to fine powder (labeled as ingredient B).

The precursors of carbon foam were prepared by adding a desired quantity of the ingredients A and B, then blending the mixture for a suitable duration (e.g. 10 min). The well-blended powder was poured into a mold as described in Fig. A1. The Kraft lignin powder in the mold was cold pressed under a pressure of 5 MPa, which was held for 30 s and a pressed Kraft lignin block was obtained (Fig. A2). The pressed lignin block in the mold was placed into a furnace and heated to 450 °C with 5 °C /min heating rate and held for 1 h. Lignin foam was formed through this pyrolysis process. After cooling to room temperature, the foam in the mold was taken out for the carbonization process, which was done in a high temperature furnace at 1100 °C for 1 h before cooling down to room temperature.

2.2. Testing of physical properties of carbon foams

2.2.1. Mechanical strength test

Compression tests were performed on lignin carbon foams based on ASTM C365 using an INSTRON 5869 mechanical testing machine [9,10]. Sample were cut into 25.4 × 25.4 × 12.5 mm size pieces and conditioned at 23 °C and 65% relative humidity for 2 weeks prior to testing. The compressive strength and compressive modulus of samples were reported.

2.2.2. Thermal conductivity measurement

The thermal conductivity of carbon foam specimens was measured using a Hot Disk TPS 1500 thermal constants analyzer (ThermTest, Fredericton, NB, Canada) following the ISO/DIS 22007–2.2 standard. A Kapton 8563 sensor was used to record the data for analysis. Measurement time ranged from 40 to 80 s. All samples were conditioned in a room held at 23 ± 1 °C with relative humidity of 65 ± 2% for two weeks until stability prior to test. The laboratory temperature was 23 ± 1 °C with relative humidity of 65 ± 2% during the measurements. Three replicates of each formulation were produced, and the average values and standard deviations were reported.

2.2.3. Electrical conductivity test

The electrical conductivity of the lignin carbon foams was evaluated by the Van der Pauw's four probe technique under atmosphere condition. Electrical contacts were made using Pt wires and Ag paste placed over whole end faces to ensure homogeneous current flow. The conductivity (σ) was calculated from a set of *V–I* values through the equation of $\sigma = 1/\rho = L/A \times dI/dV$, where *L* is the distance between voltage contacts and *A* is the sample cross section. A current load of 25–100 mA was employed with a DC/AC current source. The resultant voltage change was recorded with a voltmeter.

2.3. Termite testing

2.3.1. Preparation of test specimens

Test specimens of lignin carbon foam and Kraft lignin only blocks were cut into cubes (25 × 25 × 25 mm) and gently sanded to smooth external surfaces. Prior to testing, all sides of each specimen were imaged for use later in determining areas of termite feeding/tunneling. Test cubes were then air dried on a metal screen in a fume hood for one week. Test specimens, along with small, (25 × 25 × 4 mm) southern yellow pine (SYP) feeder blocks that will serve as termite food, were conditioned at 27 °C/30% relative humidity and weighed. Southern yellow pine feeder blocks were then joined to a corresponding lignin carbon foam block with a small rubber band prior to being placed in the testing arena.

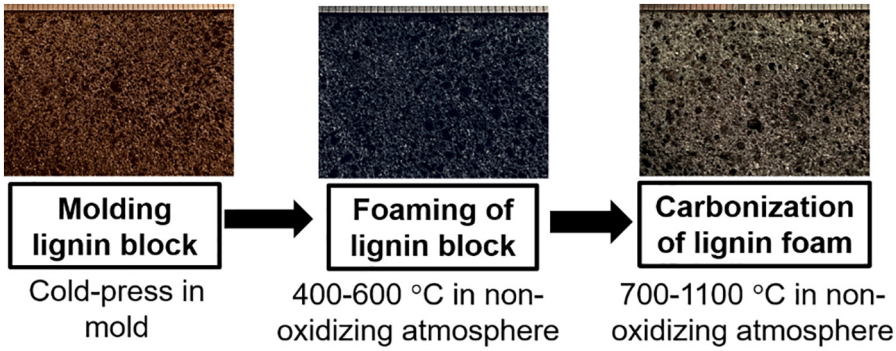

Scheme 1. Fabrication process of carbon foams from Kraft lignin.

2.3.2. Termite test set-up

Test samples ($n = 5$ per treatment) were exposed to termites in a no-choice test within a plastic jar containing sifted, sterile sand (150 g) and sterile distilled water (20 mL). The test block with attached SYP was placed on top of the sand as shown in Fig. A3. One gram of eastern subterranean termites (*Reticulitermes flavipes* (Kollar)) was added to each jar and maintained at 27 °C/90% relative humidity for the four-week testing period.

2.3.3. Evaluation of termite feeding

At the end of the test, samples were removed from the plastic jar, separated from the SYP wood feeder block, and gently brushed free of debris. Termite mortality was estimated visually for each jar. Southern pine feeder blocks were re-conditioned at 27 °C/30% relative humidity and then re-weighed to evaluate the level of termite feeding activity. Each of the lignin carbon foam blocks were visually examined for termite activity, re-imaged, and weighed.

Information of the "Kraft lignin materials", "Analysis and characterization of Kraft lignin", and "Analysis and characterization of carbon foams" details were presented in the "Supplementary Information".

3. Results and discussion

3.1. Analysis of Kraft lignin

TG and DTG curves for thermal decomposition of the Kraft lignin are shown in Fig. 1. The TG/DTG curves obtained for Kraft lignin show five-stage decomposition in the study temperature range (30–1000 °C). The first stage (30–105 °C) is characterized by a mass loss due to evaporation of physically adsorbed moisture; the peak temperature of this stage was 72.5 °C and the mass loss was 0.6%. The second stage (105–215 °C) shows a peak temperature of 180.0 °C, which is mainly attributed to dehydration of chemically bonded water and hydroxyl groups in lignin, resulting in a mass loss of about 5.5%. According to the FTIR results (Fig. A4a), the band associated with hydroxyl groups was attenuated significantly due to dehydration reactions when lignin was heated at 200 °C, while other functional groups remained unchanged. The third stage (215–290 °C) demonstrates a minor shoulder peak at about 285.5 °C which is attributed to the partial decomposition of carboxylic and anhydride groups [11] and the decomposition of the residual hemicellulose in Kraft lignin [12]. The mass loss recorded during this stage (215–290 °C) was about 6.7%. The maximum mass loss (43.1%) was observed between 290 and 600 °C which corresponded to the pyrolysis of lignin foam. According to the FTIR results (Fig. A4), most of the functional groups in the lignin basic units were decomposed. The mass decreased rapidly due to breakage of ether bonds and C—C bonds connected on the phenyl propane units, and many small molecule gases, condensable volatiles, and solid char were simultaneously generated [13]. Lignin foam is pyrolyzed to char foam in this stage. The peak of the fourth stage occurred at 390.2 °C. Lignin char foam is carbonized gradually with the temperature increasing further from 600 to 1000 °C and carbon foam is achieved when the char foam is heated at high temperature for enough time. The weight loss between 600 and 1000 °C was 6.9%.

Kraft lignin was analyzed using DSC in a temperature range of 105 to 300 °C to further understand its thermal properties. The DSC curve of the Kraft lignin is plotted in Fig. 2. The first endothermic peak at around 110.9 °C is attributed to the removal of moisture when the sample was heated. DSC was used to determine the glass transition temperature (T_g) of the Kraft lignin. Tg is an important thermal property of lignin, however, it is not easy to obtain an accurate value due to the inhomogeneous chemical structure and composition of the extracted lignin [14]. The Tg was defined as the mid-point of the temperature range at which the change in heat capacity occurs as shown by the arrow mark on the DSC-curve. It was observed that the glass transition temperature of the Kraft lignin was 146.5 °C, which is similar to the value reported by Chen et al. [15]. With increasing temperature after the glass transition, Kraft lignin starts to melt and/or soften under heat treatment [16]. The endothermic heat flow maintains at a flat level between 1.23 and 1.30 mw/mg when the heating temperature increases from 152.5 to 184.1 °C; glass transition of Kraft lignin is completed within this temperature range [16].

Kraft lignin shows a fast decline of endothermic heat flow from 1.23 mw/mg at 204.5 °C to 0.90 mw/mg at 219.5 °C due to the softening of the lignin [17]. Lignin in raw lignocellulosic materials usually does not melt under heat treatment [18]; it will pyrolyze to char or carbon materials at high temperature. However, the isolated lignin fractions with a structure similar to a linear polymer, showed good melt stability [19]. Kraft lignin from pulping processes was reported to melt at around 210 °C due to its more linear fractions and less cross-linked structures [16].

Considering the FTIR (Fig. A4) and TGA (Fig. 1) results, dehydration of hydroxyl groups accompanies the glass transition and melting/softening during heating treatment of Kraft lignin. About 5.5% of Kraft lignin mass was lost in the temperature range of 105–215 °C which is mainly the result of dehydration of chemically bonded water and hydroxyl groups in lignin. The endothermic heat flow of DSC was also partially consumed by the dehydration reaction because the moisture generated from the dehydration process is first captured in the microstructure of

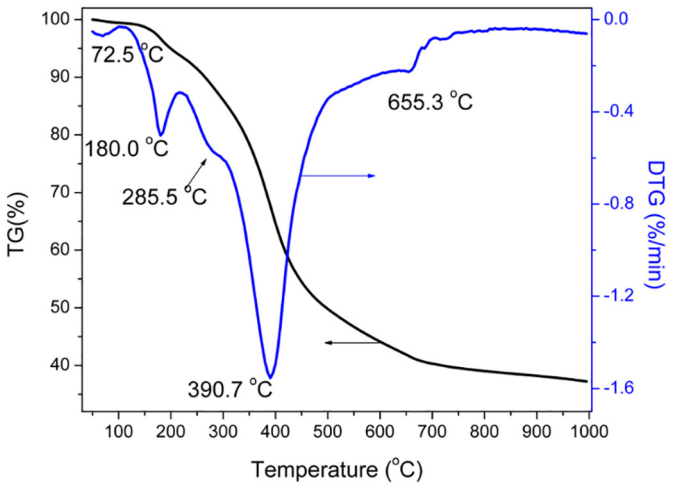

Fig. 1. TG/ DTG curves of kraft lignin.

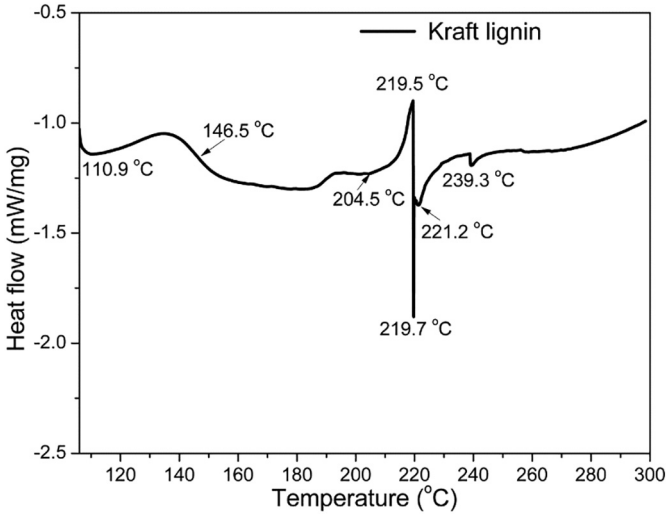

Fig. 2. DSC curve of BioChoice Kraft lignin.

the lignin block. The moisture is vaporized with increasing of the heating temperature, generating bubbles in the melted/softened lignin matrix. With further increases in the heating temperature, more moisture will be released by the dehydration process and the steam bubbles in the melted lignin expand. At the same time, the viscosity of the melted/softened lignin decreases, causing the bubbles to break through the lignin block when the steam pressure in the bubbles is high enough. DSC curve of the Kraft lignin shows the endothermic heat flow increases steeply from 0.90 mw/mg at 219.5 °C to 1.88 mw/mg at 219.7 °C and 1.37 mw/mg at 221.2 °C. The heat flow changes in the temperature range of 219.5 to 238.0 °C can be attributed to the steam bubbles breaking through the melted/softened lignin block; consequently, interconnected gas channels are created in the lignin matrix. The tiny endothermic peak at 239.3 °C is related to the decomposition of the residual hemicellulose in Kraft lignin [20]. After the degradation of hemicellulose, the endothermic heat flow decreases gradually with increasing of heating temperature, indicating the Kraft lignin decomposes slowly as the temperature increases.

To further understand the foam formation and foam carbonization process, gaseous and volatile products from pyrolysis of lignin were quantitatively and qualitatively analyzed using an on-line RGA. Fig. 3 shows the typical trends of gases released during temperature-programmed decomposition of the lignin sample. The five main gases analyzed are H_2, CH_4, CO, H_2S, and CO_2. No H_2, CH_4, or H_2S were detected, and only traces of CO_2 and CO were observed to release at temperature below 300 °C. The evolution of CO_2 started at approximately 191.3 °C and increased with increasing temperature; the formation rate was about 0.05 mL/min at 300 °C for Kraft lignin, and was mainly a result of the breaking of carboxyl groups in the phenylpropane side chains [21]. CO evolution was detected over 277.7 °C, with a formation rate of 0.01 mL/min at 300 °C. The releasing of carbon monoxide at 300 °C was contributed by the breaking of carboxyl and anhydride groups. From TGA results (Fig. 1), there is about 13% mass loss from Kraft lignin when heating in the range of 30–300 °C. After comparison to FTIR results (Fig. A4), it is concluded that the backbone structure of Kraft lignin is almost unchanged; therefore, the mass loss of the Kraft lignin sample is mainly attributed to evaporation of adsorbed water and dehydration of hydroxyl groups in lignin [22].

With further elevating the temperature of the lignin sample in the range of 300–600 °C, H_2S, CH_4 and H_2 start to be released. H_2S in trace amounts is detected from 299.1 °C (Fig. 3b) and is assigned to the decomposition of sulfide groups in the temperature range of 299–465 °C with a peak temperature at 350.9 °C (Fig. 3a). CH_4 from decomposition of Kraft lignin is observed beginning at 306.7 °C (Fig. 3b) and there are three evolution peaks at 420.3, 564.6 and 703.6 °C [23,24].

Gaseous products produced through further heating the Kraft lignin from 600 to 1100 °C are mainly composed of H_2 and CO, but also includes small amounts of CH_4 and CO_2. Heating Kraft lignin at temperatures over 500 °C eliminates hydrogen of C—H in aliphatic CH_x (x = 1–3) and aromatic rings via thermal dissociation [25]. The higher temperature CO evolution was mainly due to the cleavage of aromatic bonded oxygens (i.e. methoxy and phenolic groups) and the secondary cracking of oxygenate volatiles and tars [26,27].

In order to obtain quantitative parameters related to the formation of lignin carbon foam, the amount of gases which evolve from the carbon material between room temperature and 1100 °C was integrated and the results are listed in Table A3. Oxygen components are mainly eliminated as CO, CO_2 and H_2O during the pyrolysis and carbonization processes, while hydrogen atoms in Kraft lignin are released as H_2, CH_4 and H_2O. About 63% of the mass of Kraft lignin was lost as gaseous/volatiles products.

3.2. Formation and structure of carbon foams from Kraft lignin

TGA and gas evolution results show 45.5 wt% of raw Kraft lignin (component A) is decomposed and released as gaseous products at 450 °C which is unfavorable to form high quality carbon foam, moreover, raw Kraft lignin shows high fluidity during the heating process which is also detrimental for carbon foam formation. To reduce the fluidity and mass loss of the lignin precursor during the foaming process, Kraft lignin is partially decomposed and is added to raw Kraft lignin to prepare the foam precursor. The yield of carbon foams prepared using various component A (fresh Kraft lignin) to component B (pre-decomposed Kraft lignin at 450 °C) weight ratios are listed in Table 1. The carbon yield is in the range of 29.8–46.1 wt% when the component B weight ratio increases from 0 to 60 wt%. The gas evolution and TGA results indicated the raw Kraft lignin dominated the weight loss through thermal decomposition and the major thermal decomposition occurs before 450 °C. Less weight loss is due to the carbonization step, comprising only 15.8–15.9% weight loss for all the samples regardless of precursor composition. The precursor composition dominated the bulk density of the lignin carbon foam, with bulk density increasing from 0.18 g/cm^3 to 0.68 g/cm^3 when increasing component B ratio from 0% to 60% in the precursor. The porosity and open-cell rate of carbon foams were calculated based on bulk density, true density, and true density of pulverized foam [28]. The porosity of carbon foam decreases from

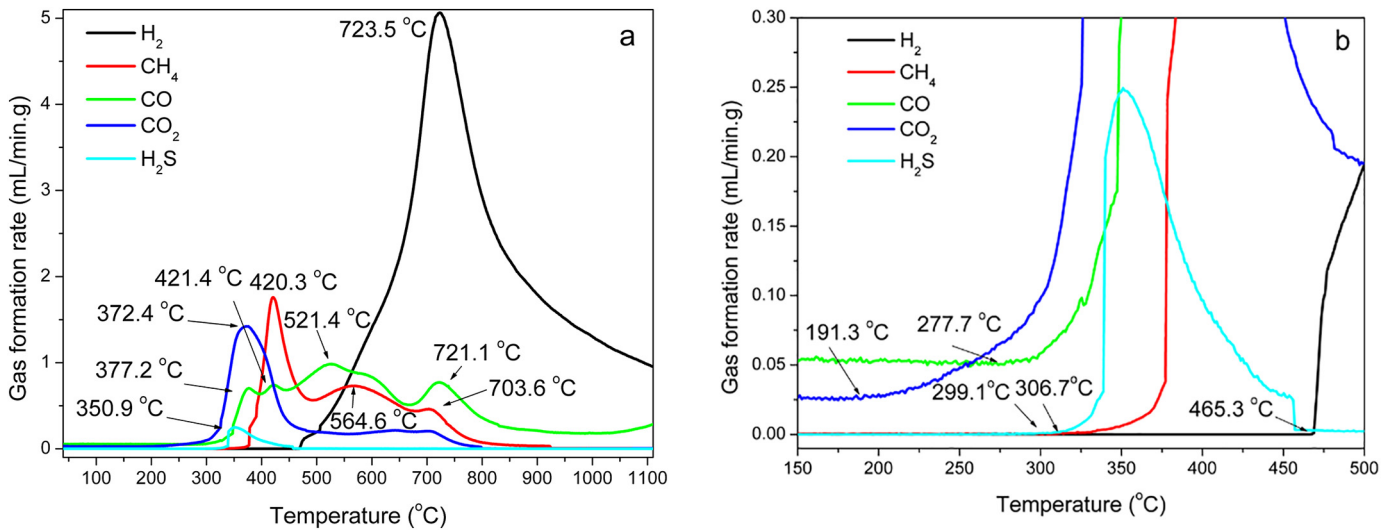

Fig. 3. Evolution of gas products from thermal decomposition of Kraft lignin (a), and partially enlarged view of a (b).

Table 1
Precursor composition, carbon foam yield, bulk density, porosity, open cell rate, and average pore size of carbon foam.

Sample ID	Ingredient A (wt%)	Ingredient B (wt%)	25–450 °C Foam formation weight loss (%)	450–1100 °C Carbonization weight loss (%)	Carbon foam yield (%)	Bulk density (g/cm^3)	Porosity (%)	Open cell rate (%)
LCF1	100	0	54.3	15.9	29.8	0.18	91.5	95
LCF2	90	10	51.5	15.8	32.5	0.21	90.1	96
LCF3	80	20	50.1	15.8	34.1	0.25	88.3	96
LCF4	70	30	46.6	15.9	37.5	0.3	86.0	97
LCF5	60	40	44	15.8	40.2	0.37	82.8	97
LCF6	50	50	41.3	15.8	42.9	0.55	75.1	98
LCF7	40	60	38.1	15.8	46.1	0.68	69.3	98

91.5% of LCF1 to 69.3% of LCF7. All these carbon foams have over 95% open-cell structure which is independent of precursor composition.

3.3. Analysis and characterization of lignin carbon foams

A summary of the C-H-O and ash elemental analysis data performed on LCF samples is shown in Table 2. The weight percentages of carbon in LCF samples were in the range of 96.7–97.4%. Hydrogen weight percentages in the carbon foam samples were all around 0.5%. Ash contents in the samples increase from 0.6% for LCF1 to 1.0% for LCF7. Oxygen contents, calculated from difference, range from 1.5–1.7%.

Fig. 4 shows XRD patterns of the lignin-derived carbon foams at different pyrolysis/carbonization temperatures. Two broad diffraction peaks, around 23.5 °C and 43.3 °C, were detected for the samples prepared in the temperature range of 600–900 °C and are attributed to the reflections of the (002) and (100) planes of amorphous carbon. The diffraction peaks of (002) and (100) shift slightly with increased temperature due to a rearrangement of carbon atoms in the carbon foam structure. As the temperature increases to 1000–1100 °C, the (002) peak shifts to 25.4–25.5 °C and becomes sharper and narrower due to the partial graphitization of carbon foam at higher temperature. The interlayer spaces between two adjacent carbon sheets (d_{002}) and the coherent domain size along the *a*-axis and *c*-axis (L_a and L_c) were calculated using Bragg's law and the Scherrer formula, respectively (Table A4). The values of d_{002} (the interlayer spacing), calculated with the Bragg equation, decreased from 0.362 to 0.337 nm as the temperature increased. This suggests an increased degree of graphitization and that the stacking of layers in the carbon foam prepared from Kraft lignin becomes more ordered at higher temperature. The d_{002} values of all the carbon foam samples are larger than 0.335 nm (graphite lattice distance), indicating the structure of the carbon foam sample is majorly turbostratic in nature despite being partially graphitized [29]. The average lateral sizes (L_a) and stacking heights (L_c) of the layer structures increase steadily with increasing temperature, demonstrating that the thickness of the stacked structure increases and the amorphous structure in carbon foam becomes ordered along both the c-axis and a-axis. The values of L_a and L_c calculated using the Bragg equation ranged from 0.891–1.336 nm and 0.951–1.709 nm, respectively as the temperature increased from 600 to 1100 °C. The graphitic structure in the carbon foam is developed gradually during the carbonization process at high temperature.

Raman spectra of lignin carbon foams were collected to study the structural evolvement with increasing temperature. Fig. 5 displays the Raman spectra of lignin carbon foams prepared at different carbonization temperatures. Two distinct bands centered at 1340 and 1590 cm^{-1} were observed for all samples. The peak at 1340 cm^{-1} is assigned to the D-band related to disordered carbon and the G-band at 1590 cm^{-1} is contributed by the sp^2 carbon in-plane vibration of graphite layers and the crystalline graphite. It is noticed the G- and D-bands are all partially overlapped for the carbon foam samples prepared at temperatures between 600 and 1100 °C, and the development of both bands becomes less overlapped with increases in temperature. The calculated values of A_D/A_G decrease from 2.64 to 1.95 as temperature increased from 600 to 1100 °C, indicating disorder carbon is the main structure of carbon foams and the graphitic structure is developed weakly with the evolution of temperature. A band at 2700 cm^{-1} was observed for the carbon foam samples prepared at 1000 and 1100 °C. This 2D band is due to crystalline graphite structure and indicates the ordered graphitic domain begins to form in the carbon foam matrix at temperatures over 1000 °C, which agrees with the XRD results (Fig. 4). The I_D/I_G values increase with increasing temperature from 600 to 1000 °C, then decrease when temperature increases to 1100 °C. This I_D/I_G trend is similar to the results reported by Fromm et al. [30].

SEM images of lignin carbon foams prepared from various ratios of Kraft lignin precursors are shown in Fig. 6. Fig. 6a shows carbon foam (LCF1) derived from raw Kraft lignin (100% A): macropores (cells) are surrounded by carbon walls (ligaments) and most of the cells are connected through holes (windows) formed in the carbon wall (i.e. an

Table 2
Summary of weight percentages (wt%) of C, H, O, and ash in the LCF samples carbonized at 1100 °C for 1 h.

Sample ID	C (%)	H (%)	O[a] (%)	Ash (%)
LCF1	97.4 ± 0.4	0.5 ± 0.1	1.5 ± 0.3	0.6 ± 0.1
LCF2	97.2 ± 0.5	0.5 ± 0.2	1.6 ± 0.2	0.7 ± 0.2
LCF3	97.2 ± 0.3	0.5 ± 0.1	1.6 ± 0.3	0.7 ± 0.1
LCF4	97.0 ± 0.5	0.5 ± 0.1	1.7 ± 0.2	0.8 ± 0.2
LCF5	97.1 ± 0.4	0.5 ± 0.2	1.6 ± 0.2	0.8 ± 0.3
LCF6	96.8 ± 0.5	0.5 ± 0.2	1.7 ± 0.2	0.9 ± 0.1
LCF7	96.7 ± 0.4	0.5 ± 0.2	1.7 ± 0.2	1.0 ± 0.1

[a] Calculated from difference: O% = 100%-C%-H%-Ash%.

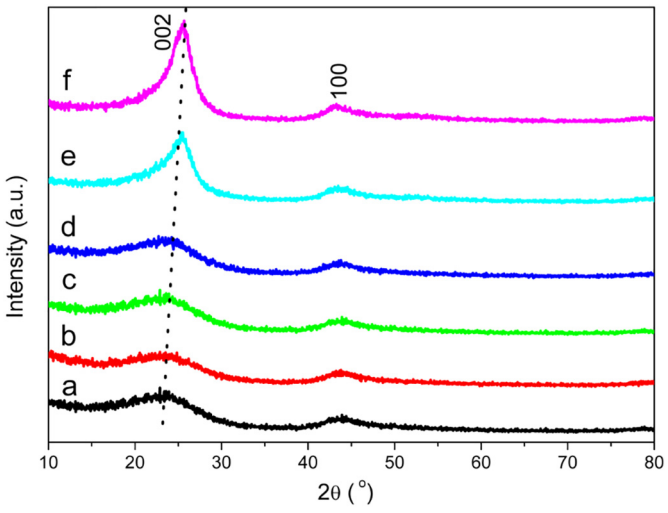

Fig. 4. X-ray diffraction patterns of lignin carbon foams synthesized under different pyrolysis/carbonization temperatures: 600 °C (a), 700 °C (b), 800 °C (c), 900 °C (d), 1000 °C (e), and 1100 °C (f).

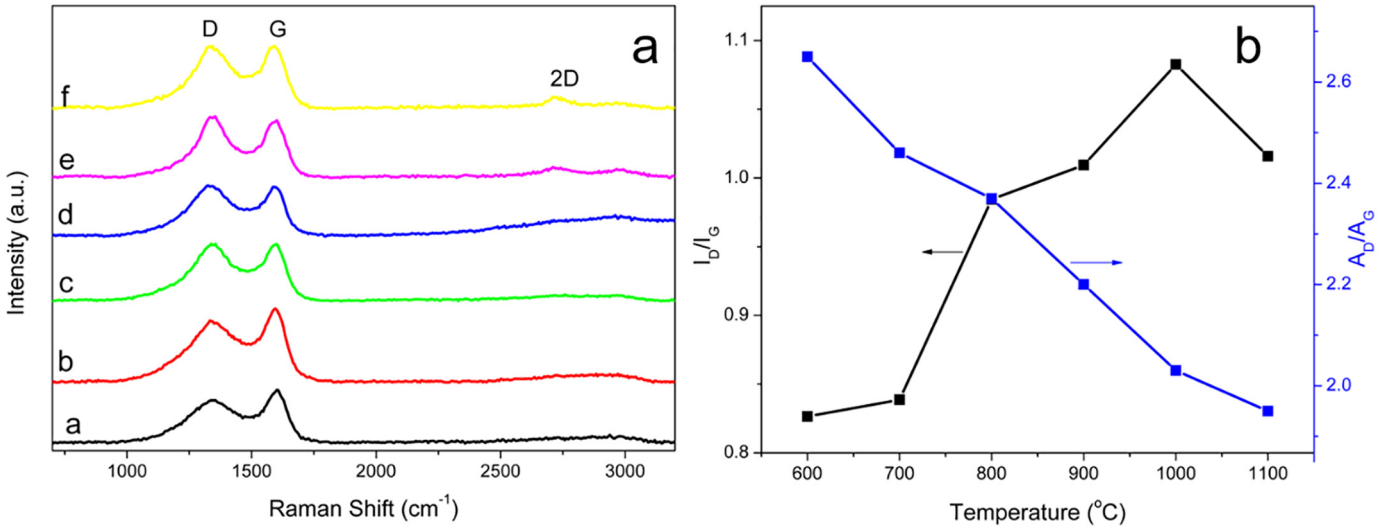

Fig. 5. Raman analysis of lignin carbon foam samples: (**a**) Raman spectra for lignin carbon foams synthesized under different pyrolysis/carbonization temperatures: 600 °C (a), 700 °C (b), 800 °C (c), 900 °C (d), 1000 °C (e), and 1100 °C (f); (**b**) the height ratio I_D/I_G and the area ratio A_D/A_G.

open cell structure for the carbon foam). The cell size is around 100–1000 μm for the LCF1. The wall of cells is made of two parts: "cell wall" and "strut" (the junction). The thickness of the cell wall is about 5–10 μm. Fig. 6b–c show the images of carbon foams (LCF2 and LCF3) prepared with precursor compositions of 90%A-10%B, and 80%A-20%B, respectively. The foam structure of LCF2 and LCF3 samples are similar to that of LCF1. Fig. 6d shows the foam structure of LCF4 (precursor 70%A-30%B). This image shows most of the cells are becoming irregular in shape, the average cell size decreases to 100 μm, and the cell wall thickness increases to 30–100 μm which is different from that of LCF1, LCF2 and LCF3. Fig. 6e–g show images of carbon foams (LCF5-LCF7) prepared with precursor compositions of 60%A-40%B, 50%A-50%B, and 40% A-60%B, respectively. It is observed that the cell structures are all irregular in shape and, with increases in the proportion of component B, cell size decreases, cell wall thickness increases, and dense struts are formed. Component B is prepared by pyrolyzing Kraft lignin at 450 °C, most of the oxygen-containing functional groups has been decomposed, consequently, less gaseous product formed during heating process, moreover, component B (lignin char) contains pores which serve as channels to release gaseous products when foaming the lignin block; therefore, with increasing of component B, less and smaller bubbles will form in the lignin foam; and a more dense product is obtained for the foam prepared with higher B component. This observation agrees with the bulk density and porosity results shown in Table 1.

3.4. Possible Kraft lignin foaming and stabilization mechanism

Scheme 2 represents an illustration of the possible foaming mechanism of Kraft lignin as revealed by results from FTIR, TGA, TPD, DSC, and SEM analyses.

The compressed lignin block in the mold may undergo the following steps: (i) the lignin molecules will swell when heated from room temperature to 140 °C [31] and the physical adsorbed moisture is desorbed as shown in TGA and DSC results (Figs. 1 and 2); (ii) after reaching the glass transition temperature (146.5 °C) as depicted by the DSC curve, the lignin block undergoes the softening/melting process where some hydroxyl groups in the lignin are concurrently dehydrated and released as moisture in the lignin matrix (supported by TGA and FTIR results) which is vaporized in the softened lignin block, resulting in steam vesicles filling the softened lignin [31] as the heating temperature increases from 140 to 219 °C; (iii) increasing the heating temperature further, more hydroxyl groups are dehydrated to form steam, causing the steam bubbles in the softened lignin to continue expanding while the viscosity of the melted/softened lignin decreases; this makes the bubbles break through the lignin matrix when the steam pressure in the bubbles is high enough (DSC data, Fig. 2), resulting in a softened lignin foam with interconnected gas channels; (iv) when the heating temperature increases above 278 °C, Kraft lignin shows obvious decomposition, releasing significant amounts of CO_2, CO, H_2S and CH_4, which are products formed from cleavage of the side chains (Fig. 3). Dehydration and side chain decomposition then lead to some crosslinking polymerizations in the lignin matrix [32]. More high molecular weight fractions are formed, causing the increase in viscosity of the lignin block and solidification of the lignin foam is initialized. The elimination of side chains mainly occurs between 278 and 450 °C with the maximum decomposition rate at 390.7 °C (i.e. more than 34% mass loss from Fig. 1). With the cleavage of the side chains, lignin molecules are condensed to form aromatic structures [33], therefore, the solid lignin foam product at 450 °C is mainly composed of aromatic clusters [34]. The foam matrix becomes more rigid and stabilized as temperature increases from 278 °C to 450 °C. The pores and the interconnected channels in the lignin matrix are further developed in this step and the solid lignin char foam is produced for further carbonization.

3.5. Main physical properties of the lignin carbon foam

3.5.1. Mechanical properties

The mechanical properties of LCF materials are complicated and depend on the initial precursor compositions, densities of the foams, and the microstructural arrangement in the foams. Fig. 7 illustrates the relationship between compressive strength and the corresponding bulk density of lignin carbon foams derived from different precursor compositions. Results showed that as the ratio of component B increased in lignin precursor composition, the bulk density of lignin carbon foam increased from 0.18 g/cm^3 (LCF1) to 0.68 g/cm^3 (LCF7). The compressive strength is found to increase with the bulk density, from 7.03 ± 1.25 MPa of LCF1 to 30.16 ± 2.41 MPa of LCF7. It is reported that cell structure of carbon foam significantly affects its mechanical strength. The cell structure parameters (the thickness of cell wall, *t*, and the length of the cell edge, *l*) and density were related by the following equation [35]:

$$(t/l)^2 \propto D_b/D_t$$

where *t* is thickness of the cell wall, *l* is length of the cell edge, D_b is bulk density, D_t is true density, and D_b/D_t is relative density.

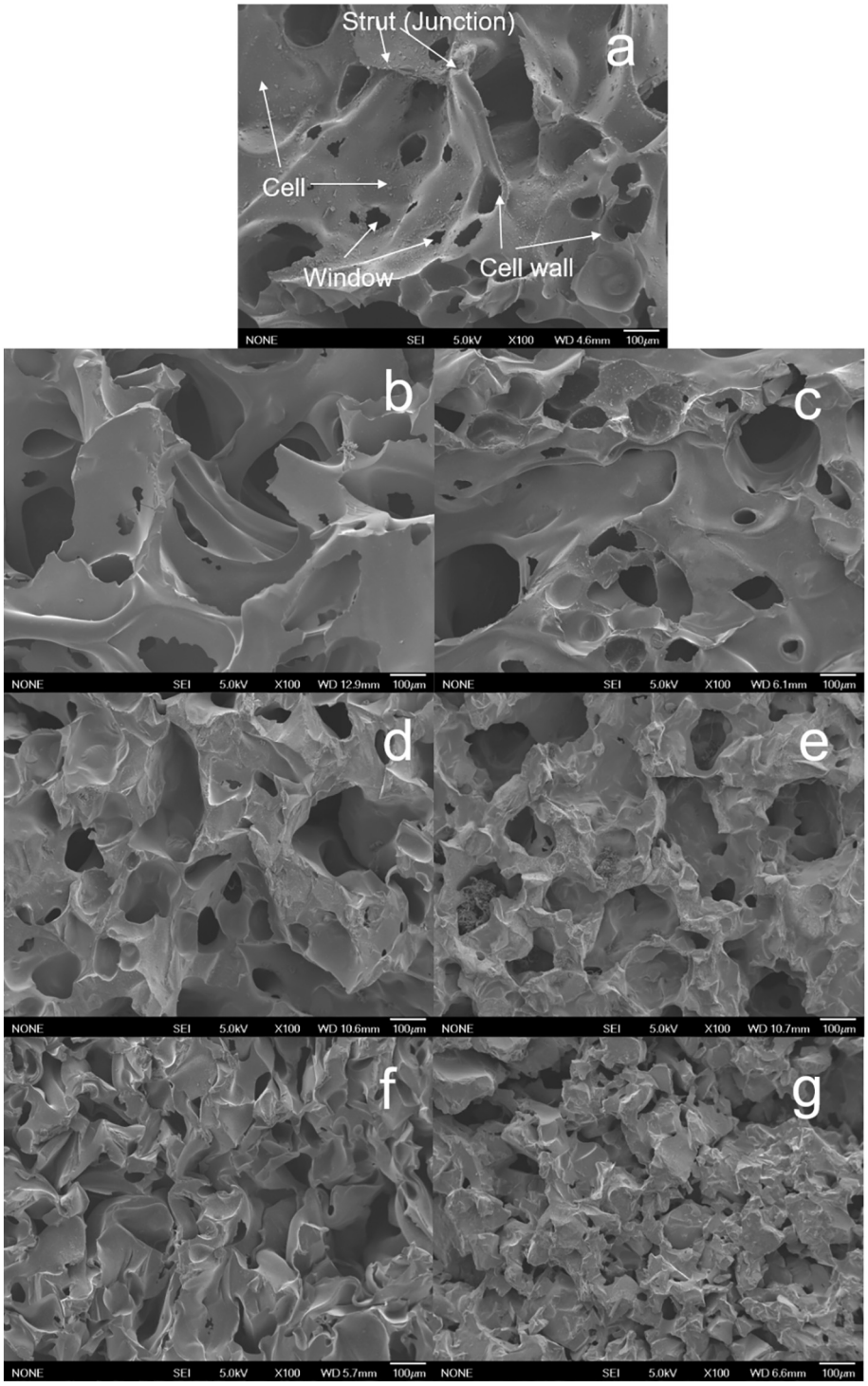

Fig. 6. SEM images of carbon foams derived from various precursor ratios: LCF1 (a), LCF2 (b), LCF3 (c), LCF4 (d), LCF5 (e), LCF6 (f), and LCF7 (g).

The increase in bulk density implies an increase in the thickness (t) of the cell wall or a decrease in the length (l) of the cell edge as a thicker cell wall and shorter cell edge promote higher compressive strength. SEM images show that the cell size (the length of the cell edge, l) decreases and the cell wall thickness (t) increases, with an increased proportion of component B, which agrees with compressive strength results.

3.5.2. Thermal conductivity

The thermal conductivity of lignin carbon foams was tested. The relationship between thermal conductivity and bulk density of foam samples is shown in Fig. 8. Thermal conductivity of a carbon foam is usually affected by the density, porosity, and fillers of the foam materials [36]. Fig. 8 indicates that the thermal conductivity of LCF samples is strongly influenced by bulk density, as thermal conductivity increases with increasing density for the foaming samples from the Kraft lignin precursor [37].

3.5.3. Electrical conductivity

The bulk electrical conductivity of lignin carbon foams, measured by the four-probe method, are plotted in Fig. 9. The bulk electrical conductivities of LCF1-LCF7 were found to increase with increasing bulk

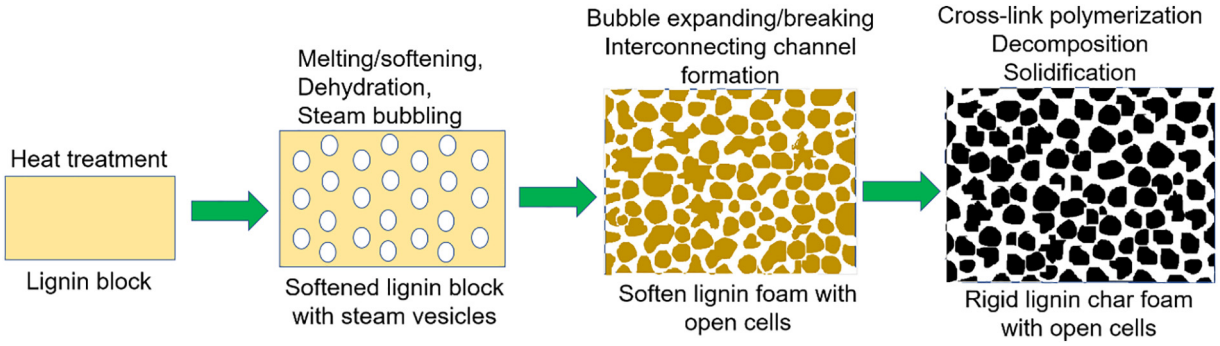

Scheme 2. Scheme of possible foaming mechanism of Kraft lignin by a heating process.

density. The electrical conductivities of LCF samples increase with bulk densities because higher density makes it easier to transfer electrons [38]. The electrical conductivity results demonstrate a trend similar to that of thermal conductivity when foam density is increased. This observation strongly supports the previous assumption that heat and current use the same pathway for traversing the material [39].

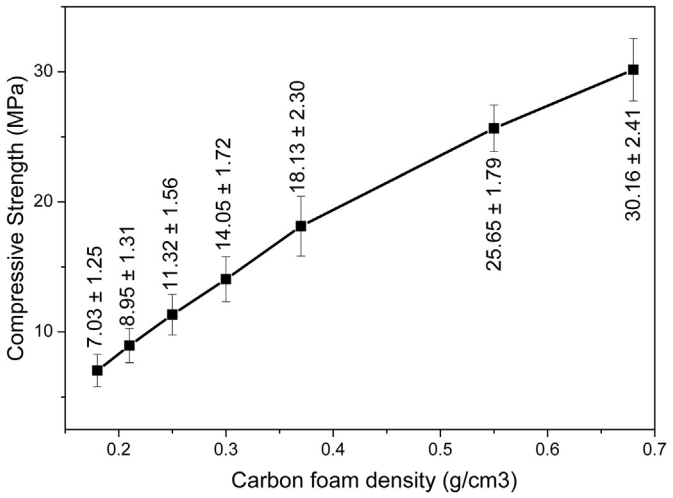

Fig. 7. Relationship of compressive strength with bulk density of LCF samples.

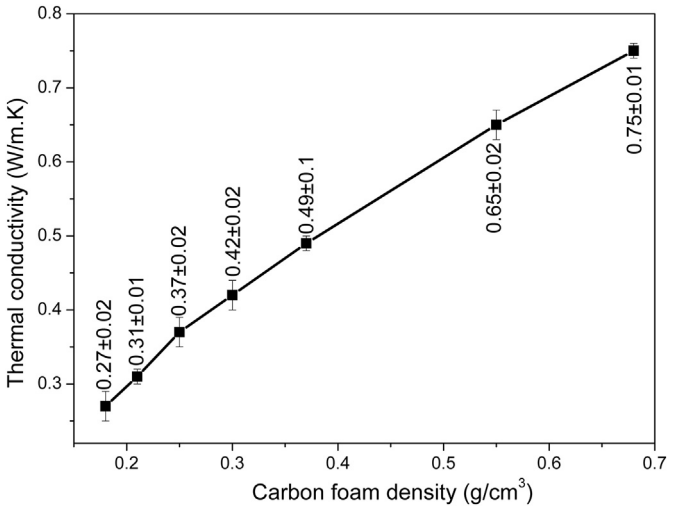

Fig. 8. Relationship between thermal conductivity and bulk density of LCF samples.

3.6. Fire resistance

Resistance of lignin carbon foam to combustion and heat when exposed to an acetylene/air flame over 1050 °C is illustrated in Fig. A5. Results show LCF samples were not ignited by fire and the flame could not burn the samples. No damage occurred when heating the LCF sample with a flame greater than 1000 °C for more than 3 min (Supplementary Video 1). Similar to carbon foams derived from bituminous coal extracts [40] and Tannins [47], LCF samples also exhibit excellent fire resistance.

3.7. Termite testing

Termites caused little to no damage to the lignin carbon foam specimens (LCF1 and LCF2) but did cause some weight loss on the lignin only blocks (Fig. 10). The negative average weight loss on the lignin carbon foam specimens is the result of termites constructing mud tubes and pasting material on the block surface and inside available holes and crevices which was not easily removed by brushing the specimens.

Lignin only test specimens were readily damaged by termites and were the only test blocks to show measurable weight loss values. It is unlikely, however, that any of the blocks were consumed but rather used as a tunneling material and incorporated into the sand below the test block (Fig. A56). Weight loss of SYP feeder blocks was comparable between all test groups (Fig. A7). It appears that termites basically ignored the lignin carbon foam blocks, but readily consumed the associated pine feeder block as a food source. In the lignin alone group,

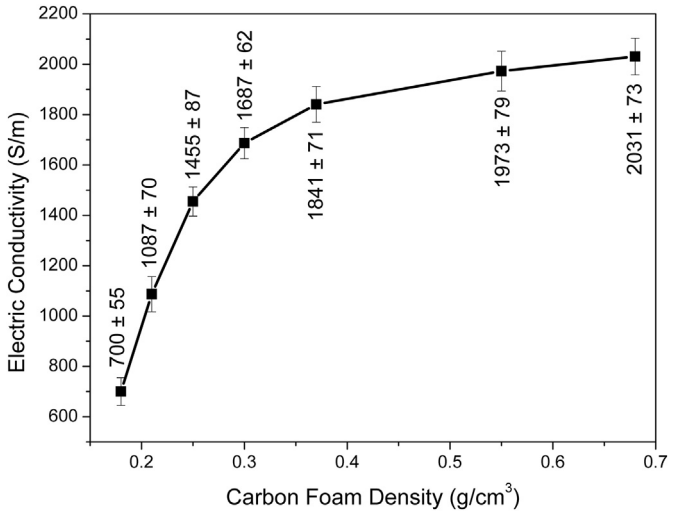

Fig. 9. Electrical conductivities of lignin carbon foams LCF1-LCF7 (electrical conductivity vs bulk density).

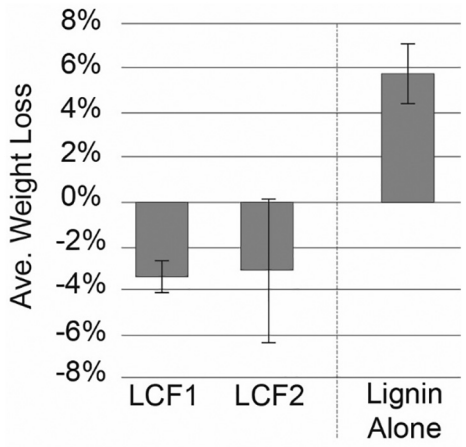

Fig. 10. Average weight loss of LCF test specimens compared to lignin alone blocks.

termites consumed less of the pine block possibly because of the low level of termite mortality in this test group.

4. Conclusions

Carbon foams were prepared from 100% Kraft lignin through a simple process: the carbon foam precursors are first compressed into a lignin block in a mold at room temperature, then the lignin block is heated to create a lignin foam block at a temperature range of 400–600 °C, and the lignin carbon foam is finally obtained by carbonization at 1100 °C. The properties obtained and structural examination showed a density of 0.18–0.68 g/cm^3; porosity of 69.3–91.5%; open-cell rate of 95%–98%; pore size ranges from 10 to 1000 μm; pore wall thickness is distributed between 10 and 100 μm; compressive strength of 7.03 ± 1.25 MPa – 30.16 ± 2.41 MPa; thermal conductivities of LCF samples increased with increasing foam bulk density; the bulk electrical conductivities of LCF samples also increased with increasing bulk density. Lignin carbon foam blocks also showed high levels of both fire and termite resistance. Fire resistance testing showed no damage occurred when the LCF sample was heated with an acetylene/air flame over 1000 °C for more than 3 min. Termite testing showed that termites ignored the lignin carbon foam blocks, but readily consumed the pine feeder block as a food source.

Supplementary data to this article can be found online at https://doi.org/10.1016/j.matdes.2021.109460.

Credit author statement

Qiangu Yan: conceptualization, experimental design and perform, original draft writing. **Rachel Arango**: termite testing design and perform, review and editing. **Jinghao Li**: investigation, sample testing, data analysis**, Zhiyong Cai**: supervision, project administration, review and editing.

Declaration of Competing Interest

The authors declare that they have no known competing financial interests or personal relationships that could have appeared to influence the work reported in this paper.

Acknowledgements

This work was supported by the USDA Forest Service through Grant Nos. 19-JV-11111124-053, 19-JV-11111124-063, 20-JV-11111124-035, and Wood Innovations Grant, No. 20-DG-11094200-234. The authors would like to acknowledge Domtar Corp., North Carolina for providing Kraft lignin for this study. Timothy Ketelboeter and Neil Gribbins at USDA Forest Products Laboratory provided editorial assistance. Special thanks to Kimberly Hoxie, Philip J. Walsh, Bruce J. Smith, CR Boardman, Sara J. Fishwild, Marshall M. Begel, James J. Bridwell, Tim Nelson, Joseph Balczewski, Joseph Destree, Will Kinney, and Randall Wruck at USDA Forest Products Laboratory, for their help in making this project run successfully.

References

[1] K.M.N. Satheesh, A.K. Mohanty, L. Erickson, M. Misra, Lignin and its applications with polymers, J. Biobased Materials. Bioenergy. 3 (2009) 1–24.
[2] Q. Yan, J. Li, X. Zhang, J. Zhang, Z. Cai, Mass production of graphene materials from solid carbon sources using a molecular cracking and welding method, J. Mater. Chem. A 7 (2019) 13978–13985.
[3] M. Mansmann, G. Winter, Production of foamed porous shaped structures of lignin suited for carbonization, US patent 3894878.
[4] D.M. Spradling, D.R. Amie, Carbon foam from metallic salts of lignosulfonates, US patent 8034266.
[5] T. Li, S. Takkellapati, The current and emerging sources of technical lignins and their applications, Biofuels Bioprod. Biorefin. 12 (5) (2018) 756–787.
[6] M.X. Wang, C.Y. Wang, T.Q. Li, Z.J. Hu, Preparation of mesophase-pitch-based carbon foams at low pressures, Carbon 46 (2008) 84–91.
[7] B. Nagel, S. Pusz, B. Trzebicka, Review: tailoring the properties of macroporous carbon foams, J. Mater. Sci. 49 (1) (2014) 1–17.
[8] L. Wang, X.T. Shi, J.L. Zhang, Y.L. Zhang, J.W. Gu, Lightweight and robust rGO/sugarcane derived hybrid carbon foams with outstanding EMI shielding performance, J. Mater. Sci. Technol. 52 (2020) 119–126.
[9] A. Standard, D695, 2010 Standard Test Method for Compressive Properties of Rigid Plastics, ASTM International, West Conshohocken, PA, 2010.
[10] A. Designation, D1621–10, Standard Test Method for Compressive Properties of Rigid Cellular Plastics, 2010.
[11] Q. Yan, J. Li, X. Zhang, J. Zhang, Z. Cai, Synthetic bio-graphene based nanomaterials through different Iron catalysts, Nanomaterials 8 (10) (2018) 840.
[12] Q. Yan, Catalytic Thermal Conversion of Kraft Lignin to Multi-Layer Graphene Materials, Ph.D. Thesis, Mississippi State University, Starkville, MS, USA, 2017.
[13] R. Bassilakis, R.M. Carangelo, M.A. Wójtowicz, TG-FTIR analysis of biomass pyrolysis, Fuel. 80 (2001) 1765–1786.
[14] S. Aminzadeh, L. Zhang, G. Henriksson, A possible explanation for the structural inhomogeneity of lignin in LCC networks, Wood Sci. Technol. 51 (2017) 1365–1376.
[15] Y. Chen, N.M. Stark, Z. Cai, C.R. Frihart, L.F. Lorenz, R.E. Ibach, Chemical modification of Kraft lignin: effect on chemical and thermal properties, Bioresources 9 (3) (2014) 5488e5500.
[16] T. Han, N. Sophonrat, A. Tagami, O. Sevastyanova, P. Mellin, W. Yang, Characterization of lignin at pre-pyrolysis temperature to investigate its melting problem, Fuel 235 (2019) 1061–1069.
[17] M.V. Ramiah, Thermogravimetric and differential thermal analysis of cellulose, hemicellulose, and lignin, J. Appl. Polym. Sci. 14 (1970) 143–1337.
[18] N.A. Nguyen, S.H. Barnes, C.C. Bowland, K.M. Meek, K.C. Littrell, J.K. Keum, A.K. Naskar, A path for lignin valorization via additive manufacturing of high-performance sustainable composites with enhanced 3D printability, Sci. Adv. 4 (12) (2018) eaat4967.
[19] W.G. Glasser, About making lignin great again—some lessons from the past, Front. Chem. 7 (2019) 1–17.
[20] H. Yang, R. Yan, H. Chen, L. Dong Ho, C. Zheng, Characteristics of hemicellulose, cellulose and lignin pyrolysis, Fuel 86 (2007) 1781–1788.
[21] E.A. Boakye, Lignin Transformation and Characterization of Pyrolytic Products, 2017 1185 , Theses and Dissertations http://openprairie.sdstate.edu/etd/1185.
[22] Q. Yan, C.R. Boardman, Z. Cai, Thermal stability of metal-lignin composites prepared by coprecipitation method, Thermochim. Acta 690 (2020) 178659.
[23] G. Wang, H. Dai, Z. Yang, Luo, Lignocellulosic biomass pyrolysis mechanism: a state-of-the-art review, Prog. Energy Combust. Sci. 62 (2017) 33–86.
[24] Q. Liu, S. Wang, Y. Zheng, Z. Luo, K. Cen, Mechanism study of wood lignin pyrolysis by using TG–FTIR analysis, J. Anal. Appl. Pyrolysis 82 (2008) 170–177.
[25] M. Brebu, C. Vasile, Thermal degradation of lignin—a review, Cellul. Chem. Technol. 44 (2010) 353–363.
[26] J. Cao, G. Xiao, X. Xu, D. Shen, B. Jin, Study on carbonization of lignin by TG-FTIR and high-temperature carbonization reactor, Fuel Process. Technol. 106 (2013) 41–47.
[27] S.C. Fox, A.G. McDonald, Chemical and thermal charcterization of three industrial lignins and their corresponding lignin esters, BioResources 5 (2010) 990–1009.
[28] J. Eckardt, J. Neubauer, T. Sepperer, S. Donato, M. Zanetti, N. Cefarin, L. Vaccari, M. Lippert, M. Wind, T. Schnabel, et al., Synthesis and characterization of high-performing sulfur-free tannin foams, Polymers 12 (2020) 564.
[29] M.T. Johnson, K.T. Faber, Catalytic graphitization of three-dimensional wood-derived porous scaffolds, J. Mater. Res. 26 (1) (2011) 18–25.
[30] O. Fromm, A. Heckmann, U.C. Rodehorst, J. Frerichs, D. Becker, M. Winter, et al., Carbons from biomass precursors as anode materials for lithium ion batteries: new insights into carbonization and graphitization behavior and into their correlation to electrochemical performance, Carbon 128 (2018) 147–163.
[31] B. Shrestha, Y. le Brech, T. Ghislain, S. Leclerc, V. Carré, F. Aubriet, S. Hoppe, P. Marchal, S. Pontvianne, N. Brosse, A. Dufour, A multitechnique characterization of lignin softening and pyrolysis, ACS Sustain. Chem. Eng. 5 (2017) 6940–6949.

[32] J.H. Grabber, How do lignin composition, structure, and cross-linking affect degradability? A review of cell wall model studies, Crop Sci. 45 (2005) 820–831.
[33] Z. Sun, B. Fridrich, A. de Santi, S. Elangovan, K. Barta, Bright side of lignin depolymerization: toward new platform chemicals, Chem. Rev. 118 (2) (2018) 614–678.
[34] S. Agarwal, R.K. Chowdari, I. Hita, H.J. Heeres, Experimental studies on the hydrotreatment of Kraft lignin to aromatics and alkylphenolics using economically viable Fe-based catalysts, ACS Sustain. Chem. Eng. 5 (2017) 2668–2678.
[35] S. Wang, R. Luo, Y. Ni, Preparation and characterization of resin-derived carbon foams reinforced by hollow ceramic microspheres, Mater. Sci. Eng. A 527 (2010) 3392–3395.
[36] H.G. Kim, Y.S. Kim, L.K. Kwac, S.-H. Chae, H.K. Shin, Synthesis of carbon foam from waste artificial marble powder and carboxymethyl cellulose via electron beam irradiation and its characterization, Materials 11 (2018) 469.
[37] L. Yu, Z. Feng, Z. Fan, Q. Kong, L. Xu, The preparation and properties of novel structural carbon foams derived from different mesophase pitches, 5th International Conference on Porous Media and Their Applications in Science, Engineering and Industry, 2014.
[38] Z. Sui, Q. Meng, X. Zhang, R. Ma, B. Cao, Green synthesis of carbon nanotube–graphene hybrid aerogels and their use as versatile agents for water purification, J. Mater. Chem. 22 (2012) 8767–8771.
[39] G. Tondi, V. Fierro, A. Pizzi, A. Celzard, Tannin-based carbon foams, Carbon 47 (2009) 1480–1492.
[40] D.K. Rogers, J. Plucinski, Low-cost carbon foams for thermal protection and reinforcement applications. Extended abstracts, In 45th international SAMPE symposium, May 21–25, 2000.